

This work was written as part of one of the author's official duties as an Employee of the United States Government and is therefore a work of the United States Government. In accordance with 17 U.S.C. 105, no copyright protection is available for such works under U.S. Law.

Public Domain Mark 1.0

<https://creativecommons.org/publicdomain/mark/1.0/>

Access to this work was provided by the University of Maryland, Baltimore County (UMBC) ScholarWorks@UMBC digital repository on the Maryland Shared Open Access (MD-SOAR) platform.

**Please provide feedback**

Please support the ScholarWorks@UMBC repository by emailing [scholarworks-group@umbc.edu](mailto:scholarworks-group@umbc.edu) and telling us what having access to this work means to you and why it's important to you. Thank you.

## Generation of Pi2 pulsations by intermittent earthward propagating dipolarization fronts: An MHD case study

J. B. Ream,<sup>1,2</sup> R. J. Walker,<sup>2,3</sup> M. Ashour-Abdalla,<sup>1,4</sup> M. El-Alaoui,<sup>1,4</sup> M. G. Kivelson,<sup>1,2</sup> and M. L. Goldstein<sup>5</sup>

Received 6 February 2013; revised 27 September 2013; accepted 2 October 2013; published 18 October 2013.

[1] Using a global magnetohydrodynamic (MHD) simulation of the magnetosphere during a disturbed interval on 14 September 2004, we have investigated fluctuations in plasma properties of the magnetotail in the Pi2 range and their relationship to dipolarization fronts (DFs). Results from the MHD simulation indicate that this event is a very active interval with variable convection and disorder in the tail on a range of scales as small as  $\sim 1 R_E$ . DFs are observed in the simulation at the leading edge of fast earthward flows that originate from reconnection regions that form between  $\sim -15$  and  $-30 R_E$  in the tail. Pi2 period fluctuations are identified in pressure, magnetic field, and velocity components inside  $-13 R_E$  following each burst of DFs in the midnight sector. The fluctuations observed in the pressure appear to be generated by the successive DFs as they approach the interface between stretched tail field lines and dipolar field lines. Fluctuations in the velocity may be the result of interactions between successive DFs and are amplified directly following the passage of the DFs as they propagate earthward. Although the limited azimuthal extent of the pulsations near the plasma sheet, just inside of the braking region, makes it difficult to draw a direct comparison between the ground-based measurements and the pulsations at  $-6 R_E$ , the temporal evolution of the simulated DFs and Pi2 pulsations approximately reproduces the timing of the variations observed by satellites and ground-based instruments. Therefore, we have been able to use the global simulation to track the bursty flows, dipolarization fronts, and associated Pi2 period fluctuations throughout the entire magnetosphere in order to understand the sources of the changes measured in the near-Earth region.

**Citation:** Ream, J. B., R. J. Walker, M. Ashour-Abdalla, M. El-Alaoui, M. G. Kivelson, and M. L. Goldstein (2013), Generation of Pi2 pulsations by intermittent earthward propagating dipolarization fronts: An MHD case study, *J. Geophys. Res. Space Physics*, 118, 6364–6377, doi:10.1002/2013JA018734.

### 1. Introduction

[2] The processes that occur in Earth's magnetotail during the period leading up to substorm onset are not fully understood. One of the methods used to identify the time of substorm onset is to identify the time when Pi2 pulsations begin in ground-based magnetometer records at midlatitudes

[e.g., Saito *et al.*, 1976; Sakurai and Saito, 1976; Olson, 1999; Miyashita *et al.*, 2000; Kepko *et al.*, 2004; Hsu and McPherron, 2007; Kim *et al.*, 2007; Keiling *et al.*, 2008]. Pi2 pulsations are ultralow frequency waves ( $T = 40\text{--}150$  s) that come in packets at irregular intervals. Pulsations in the same band of frequencies have been observed in magnetic field and velocity measurements at geosynchronous orbit in conjunction with dipolarization fronts [e.g., Kepko and Kivelson, 1999]. Well-correlated measurements of the phenomena have led to several theories concerning the generation of Pi2 pulsations by DFs [e.g., Kepko and Kivelson, 1999; Kepko *et al.*, 2001; Panov *et al.*, 2010; Keiling *et al.*, 2008; Murphy *et al.*, 2011]. Recently, Hsu *et al.* [2012] used a statistical study to show that 90% of plasma flows in the tail are associated with Pi2's, indicating that either the plasma flows generate the Pi2 pulsations, or that the flows and Pi2s are generated by the same process. Because midlatitude Pi2 can be used to identify the onset time of a substorm, understanding how they are generated is vital to understanding the series of events leading up to onset.

[3] Intermittent fast flows ( $|\vec{v}| > 100$  km/s), often referred to as bursty bulk flows (BBFs), are observed frequently in

Additional supporting information may be found in the online version of this article.

<sup>1</sup>Institute for Geophysics and Planetary Physics, University of California, Los Angeles, California, USA.

<sup>2</sup>Department of Earth and Space Sciences, University of California, Los Angeles, California, USA.

<sup>3</sup>National Science Foundation, Arlington, Virginia, USA.

<sup>4</sup>Department of Physics and Astronomy, University of California, Los Angeles, California, USA.

<sup>5</sup>Heliospheric Physics Laboratory, Goddard Space Flight Center, Greenbelt, Maryland, USA.

Corresponding author: J. B. Ream, Department of Earth and Space Sciences, University of California, Los Angeles, 595 Charles Young Dr. East, Box 951567, Los Angeles, CA 90095-1567, USA. (jodiebt@ucla.edu)

©2013. American Geophysical Union. All Rights Reserved.  
2169-9380/13/10.1002/2013JA018734

the tail [e.g., Scholer et al., 1984; Angelopoulos et al., 1992, 1994] and have been linked to reconnection events at neutral lines that form in the near-Earth region between  $-15$  and  $-25 R_E$  [e.g., Pytte et al., 1976; Hones et al., 1984; Angelopoulos et al., 2008; Nagai et al., 1998; Miyashita et al., 2009; Gabrielse et al., 2009]. BBFs cause an increase in thermal pressure, and a magnetic pileup and dipolarization in the plasma sheet as they travel earthward. The leading edge of the plasma sheet dipolarization is referred to as a dipolarization front (DF) and develops at the boundary between the flowing plasma and the background plasma [Runov et al., 2009, 2011]. DFs are observed as enhancements in  $B_z$  that occur over the course of a few seconds. They are typically accompanied by a drop in  $B_x$  and occur throughout the magnetotail from  $x = -5$  to  $-31 R_E$  during disturbed periods as observed by satellites and in simulations [e.g., Slavin et al., 1997; Nakamura et al., 2009; Sitnov et al., 2009; Ashour-Abdalla et al., 2011]. The dipolarization region behind a DF is sometimes referred to as an entropy bubble since it is associated with flux tubes that have decreased entropy content [e.g., Pontius and Wolf, 1990; Chen and Wolf, 1993; Sergeev et al., 1996; Chen and Wolf, 1999; Wolf et al., 2009]. As the DFs encounter the region where the magnetic field lines transition from a stretched to a dipolar configuration, there is a pileup effect in the magnetic field that causes an expansion of the region in both tailward and azimuthal directions [Hesse and Birn, 1991]. This expansion is often referred to as dipolarization associated expansion.

[4] Pi2 pulsations have been studied extensively for several decades; however, the source of the Pi2 observed on the ground is still a subject of debate [e.g., Olson, 1999; Keiling and Takahashi, 2011, and references therein]. Kepko et al. [2001] suggested that both the compression regions and time variations in velocity associated with the braking of dipolarization fronts drive Pi2 pulsations. Based on the different drivers, the authors divided Pi2 pulsations into three distinct categories: Transient Response (TR), Inertial Current (IC), and Directly Driven (DD). TR and IC Pi2 pulsations are associated with the substorm current wedge [McPherron, 1972] and arise because of an impedance mismatch between the ionosphere and magnetosphere as the DFs propagate earthward [Southwood and Stuart, 1980] and time variations in the flow velocity in the braking region, respectively. Although both the TR and IC Pi2 are observed at middle to high latitudes, they have slightly different signatures on the ground. Specifically, TR Pi2 has a damped sinusoidal form which continues after the driving flow has stopped, and IC Pi2 has a relatively constant amplitude and is only present while the flows are present. In addition, the waveforms of the IC Pi2 match the flow variations in the magnetotail while the TR Pi2 waveforms do not [Kepko and Kivelson, 1999; Kepko et al., 2001]. DD Pi2 is caused by flow variations in the radial direction due to the deceleration of earthward flows in the high pressure region near the inner edge of the plasma sheet where field lines change from a stretched to a dipolar geometry. This generates a compressional wave that travels earthward across the background magnetic field [e.g., Russell and McPherron, 1973; Chang and Lanzerotti, 1975] to generate middle to low-latitude Pi2 observed on the ground. There are several theories concerning how the compressional waves travel through the inner magnetosphere/plasmasphere including surface

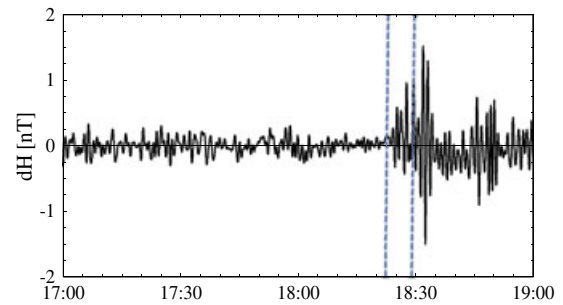


**Figure 1.** Filtered  $B_H$  from the ground magnetometer in Urumqi, China. The station is located at  $43.80^\circ$  latitude and  $87.70^\circ$  longitude, ( $33.4^\circ$  magnetic latitude). At the time of substorm onset (1828 UT) the station is located at 0222 magnetic local time (MLT).

waves traveling along the plasmopause [e.g., Sutcliffe, 1975; Southwood and Stuart, 1980] and cavity mode resonances [e.g., Saito and Matsushita, 1968; Yeoman and Orr, 1989; Sutcliffe and Yumoto, 1991; Takahashi et al., 1992]. Thorough reviews of these theories for low-latitude Pi2 are given by Olson [1999] and Keiling and Takahashi [2011].

[5] Recently, Panov et al. [2010] extended the Kepko et al. [2001] interpretation suggesting that Pi2 pulsations are generated by the overshoot and rebound of bursty bulk flows (BBFs) at the braking region causing the compressional wave to travel earthward. Murphy et al. [2011] proposed a slightly different scenario where flow variations at the BBF origin cause Alfvén-mode waves to propagate along field lines and fast-mode waves to propagate earthward in the plasma sheet ahead of the BBF. All three of the models are closely related in that they suggest that variations in the pressure and in velocity associated with the earthward propagation of dipolarization fronts generate the Pi2 pulsations measured by ground-based magnetometers.

[6] Using a global MHD simulation of a substorm event, we are able to identify the variations in the magnetic field, pressure, and velocity to determine where they originate and how they evolve as they propagate earthward. We investigate the relationship between these variations and the passage of dipolarization fronts throughout the system. The discussion in this paper is limited to IC and DD Pi2 with a focus on identifying the Pi2 pulsations near geosynchronous orbit and linking them to the Pi2 period fluctuations further out in the magnetotail.

[7] The paper is organized as follows: In section 2, we describe the satellite and ground-based observations from 14 September 2004. We describe the MHD simulation in section 3 along with a comparison of the simulation results with the satellite measurements. We discuss the identification of the dipolarization fronts and Pi2 pulsations in section 4 and show the relationship between these phenomena and how our results are related to the models presented in previous studies in section 5. We end with a summary of our conclusions in section 6.

## 2. Observations

[8] The event we have selected for this study is a moderate substorm on 14 September 2004 whose properties have previously been reported on by Cao et al. [2008, 2012] based on observations by Double Star, Cluster, Imager for

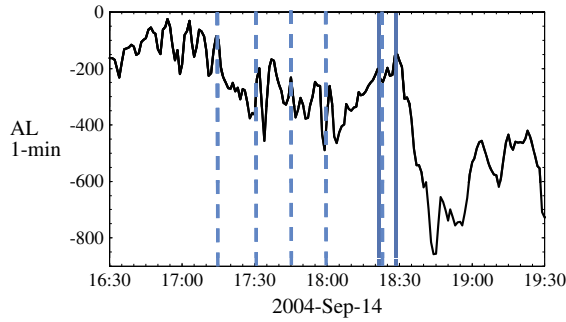


**Figure 2.** The 1 min  $AL$  index during the substorm on 14 September 2004 (1630–1930 UT) from the OMNI database (solar wind data provided by Space Physics Data Facility). The solid vertical lines indicate Pi2 onset ( $\sim 1822$  UT) and substorm onset ( $\sim 1828$  UT) as identified using ground-based magnetometer data,  $AL$  and IMAGE observations. The dashed vertical lines indicate the times when bursts of DFs are observed in the simulation.

Magnetopause-to-Aurora Global Exploration (IMAGE), and ground-based magnetometers. Pi2 onset measured by the Urumqi magnetometer (northwest China; 48 magnetic latitude (MLAT)) occurs at  $\sim 1822$  UT (first dashed line) shown in Figure 1 [http://wdc.kugi.kyoto-u.ac.jp]. The instrument observed a burst of Pi2 pulsations at  $\sim 1822$ – $1834$  UT with a smaller burst around 1845 UT. The period of the observed Pi2s is  $\sim 60$ – $90$  s. The Norlisk (NOK) magnetometer in Russia (MLAT 59.50) [Gjerloev, 2009, 2012] observed a drop of  $\sim 700$  nT in the northward component beginning at 1821 UT and confirms the Pi2 timing (not shown). The  $AL$  index [Davis and Sugiura, 1966] (Figure 2), however, shows a period of steady moderate activity between 1715 UT and 1820 UT followed by an expansion phase beginning at  $\sim 1828$  UT; 6 min after Pi2 onset. At this time, the  $AL$  index decreases sharply from  $-150$ , reaching a minimum of  $-857$

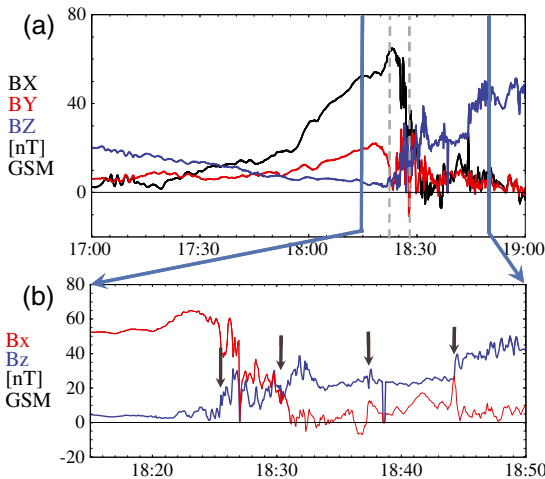


**Figure 3.** (a) Magnetic field measurements  $B_x$  (black),  $B_y$  (red), and  $B_z$  (blue) for Double Star (TC1) for the time period 14 September 2004 1500–2000 UT. Pi2 onset (1822 UT) and substorm onset (1828 UT) are indicated by the dashed gray lines. (b)  $B_z$  (blue) and  $B_x$  (red) during the interval 1815–1850 UT (indicated by the blue solid lines in Figure 3a). The arrows indicate times of DFs.

at 1844 UT. The discrepancy between Pi2 onset and the  $AL$  substorm onset could be due to the limited number of  $AL$  stations on the nightside during this event. Another possibility is that the NOK and Urumqi instruments detected a pseudobreakup with the full substorm onset developing shortly thereafter, as indicated by the  $AL$  index.

[9] Plasma sheet observations for this event are from Double Star (TC1) located at  $(-10.2, -1.6, 1.2) R_E$  GSM. The data used in this study come from the Fluxgate Magnetometer (FGM) [Carr et al., 2005] aboard the satellite. TC1 is located very close to the central plasma sheet (CPS) around the time of substorm onset, which is the ideal position to observe DFs propagating in the magnetotail. Figure 3a shows the magnetic field measurements from TC1. There is an interval from  $\sim 1755$  to  $\sim 1825$  UT when TC1 is near the edge of the plasma sheet. During this interval,  $B_x$  increases and  $B_z$  decreases. It is possible that the plasma sheet became very thin during this interval. Figure 3b expands the plots of  $B_z$  (blue) and  $B_x$  (red) for the interval between the solid blue lines (1815 to 1850 UT). Three DFs were observed by TC1 at  $\sim 1825$ , 1830, and 1844 UT, with the possibility of a fourth DF at 1837 UT. The signatures are identified as sharp jumps in  $B_z$  with corresponding decreases in  $B_x$  and are marked with gray arrows in Figure 3b. TC1 also observed Pi2 pulsations beginning at  $\sim 1821$  UT (Figure 4a), just before the first DF was observed as shown in Figure 3, and  $\sim 1$ – $2$  min before Pi2 onset on the ground. This suggests a relationship between the two phenomena.

[10] We use Geotail, which was located just outside the bow shock at  $(25, 17, -2) R_E$  GSM, as the solar wind probe for this event [Frank et al., 1994; Kokubun et al., 1994]. A small time shift ( $< 2$  min) was applied to propagate the measurements to the bow shock. Geotail measurements are shown in Figure 5. The panels show (Figure 5a) magnetic field  $B_x$  (black),  $B_y$  (blue), and  $B_z$  (red); (Figure 5b)  $v_x$ ; (Figure 5c)  $v_y$  (black) and  $v_z$  (red); (Figure 5d) density; and (Figure 5e) ion temperature. There is a period where the interplanetary magnetic field (IMF) is dominated by  $B_y$  between 1640 and 1730 UT. The IMF turns slightly southward at  $\sim 1707$  UT and  $B_z$  becomes more negative at 1730 UT. A strong northward turning occurs at  $\sim 1830$  UT, coincident with the beginning of the expansion phase in  $AL$ .

[11] Satellite- and ground-based observations for this event are discussed in detail by Cao et al. [2008]. The

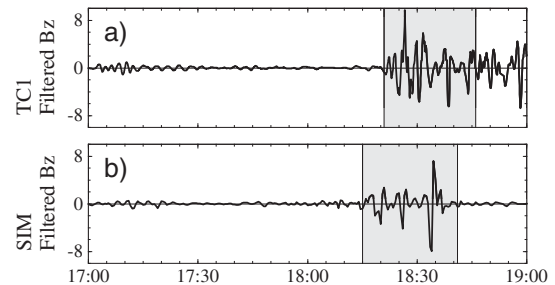


**Figure 4.** Filtered  $B_z$  for (a) TC1 and (b) simulation results near the TC1 location. The times for Pi2 onset in the two panels are offset by 5 min. The gray areas indicate times when the Pi2 in the simulation correspond to the TC1 measurements.



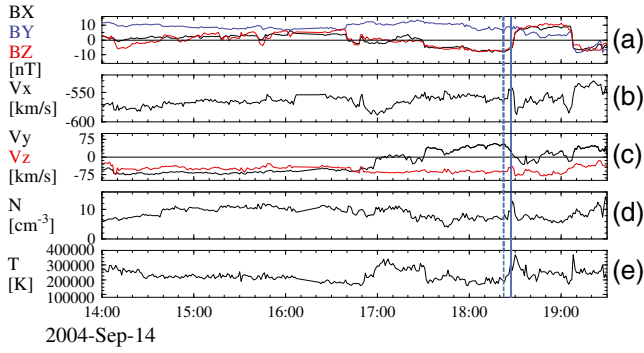


**Figure 5.** Geotail solar wind measurements for 14 September 2004 1400–1930 UT used for input in the MHD simulation. (a) Magnetic field  $B_x$  (black),  $B_y$  (blue), and  $B_z$  (red) (nT), (b) solar wind velocity  $v_x$ , (c) solar wind velocity  $v_y$  (black),  $v_z$  (red) (km/s), (d) density ( $\text{cm}^{-3}$ ), and (e) ion temperature ( $^{\circ}\text{K}$ ). Dashed blue line indicates Pi2 onset and solid blue line indicates substorm onset.

authors used the timing between observations of magnetic dipolarization at TC1 and Cluster 4 (located outside of the plasma sheet until  $\sim 1850$  UT) along with multipoint analysis techniques [Nakamura *et al.*, 2005] to show that dipolarization-related disturbances propagate tailward at a speed of  $\sim 86$  km/s. They also relate the tailward expansion of the magnetic dipolarization to poleward expansion of auroral bulges observed by the IMAGE spacecraft [Mende *et al.*, 2001]. Preonset auroral signatures for this event were investigated in depth by Cao *et al.* [2012]. In this paper, the authors discuss a double oval in the image data at 1720 UT with poleward boundary intensifications beginning at  $\sim 1752$  UT. They also point out auroral streamers in the IMAGE satellite auroral data between  $\sim 1801$  and  $\sim 1820$  UT and argue that these signatures are indicative of earthward flows during the growth phase of the substorm. However, onset for this event in the IMAGE auroral observations is not clearly defined. There is a full auroral oval that formed during an earlier substorm at  $\sim 1520$  UT. Although there was auroral brightening seen at the time of the Pi2 onset at Urumqi (1820–1822 UT), poleward expansion did not begin until  $\sim 1826$ –1829 UT. Substorm onset based on the IMAGE observations could be placed at any time between 1820 and 1829 UT.

### 3. Simulation

[12] An MHD simulation was carried out with the University of California, Los Angeles (UCLA) global MHD code to establish the magnetosphere's response to the solar wind conditions observed before and during the substorm event. The UCLA global MHD code is a coupled magnetosphere-ionosphere three-dimensional global MHD code based on a one-fluid description of the interaction between the solar wind and the magnetosphere. This code is discussed in detail by Raeder *et al.* [1998] and El-Alaoui [2001], so we will only give a brief description here. The simulation box is 20 to  $-300 R_E$  in  $x$ , and 55 to  $-55 R_E$  in  $y$  and  $z$ , GSM, and uses a nonuniform Cartesian grid with the minimum grid spacing set at  $0.15 R_E$ . The code solves the normalized resistive MHD equations on the grid. The electric field in the code includes both convective and resistive terms  $\vec{E} = -\vec{v} \times \vec{B} + \eta \vec{j}$ ,

where  $\vec{j}$  is the current,  $\vec{B}$  is the magnetic field,  $\vec{E}$  is the electric field, and  $\eta$  is the anomalous resistivity. This anomalous resistivity is defined by

$$\eta = \alpha j'^2 \quad \text{if } j' \geq \delta, \quad 0 \quad \text{otherwise}$$

$$j' = \frac{|j| \Delta}{|B| + \epsilon}$$

where  $j'$  is the normalized current density,  $\Delta$  is the grid spacing,  $j$  is the local current,  $B$  is the local magnetic field, and  $\epsilon$  is used to avoid dividing by zero. The quantities  $\alpha$  and  $\delta$  are set such that the resistivity is only nonzero in strong current sheets.

[13] The inner boundary of the simulation is a spherical shell placed at a radius of  $2.7 R_E$ . This is where the MHD variables are coupled to the ionosphere via the field-aligned currents (FAC) using the ionospheric potential equation

$$\nabla \cdot \bar{\Sigma} \cdot \nabla \Phi = -j_{\parallel} \sin I \quad (1)$$

where  $\Phi$  is the ionospheric potential as a function of magnetic latitude and local time,  $\Sigma$  is the tensor of the ionospheric conductance including Hall and Pedersen conductance,  $j_{\parallel}$  is the mapped FAC with the downward current considered positive and corrected for flux tube convergence, and  $I$  is the inclination of the dipole field at the ionosphere [Raeder *et al.*, 1998]. The conductance distribution in the model is determined by using solar EUV, as well as discrete and diffuse precipitation, self-consistently with the MHD model [Raeder *et al.*, 1998, 2001; El-Alaoui *et al.*, 2009]. Equation (1) is solved on the surface of a sphere with radius  $1.015 R_E$ , an altitude of 110 km, then mapped along field lines to the inner edge of the MHD model where it is used as a boundary condition for the flows.

[14] The sunward outer boundary conditions are set to the time-dependent solar wind conditions (magnetic field, velocity, density, and temperature) measured by Geotail during the event (Figure 5). To prepare the solar wind data for input into the simulation, Geotail magnetic field measurements for 14 September 2004 are rotated into a minimum variance frame. The normal component of the magnetic field is then set to a constant. The method outlined here is used to propagate the solar wind parameters from Geotail to the inflow boundary and keeps divergence of  $\vec{B}$  equal to zero throughout the simulation [El-Alaoui, 2001]. Open (i.e., zero normal derivative) boundary conditions are applied to all other outer boundaries. Output for this simulation was captured every 30 s between 1400 and 1927 UT.

### 4. Simulation Results

[15] In order to observe structures propagating along the plasma sheet, it is useful to remove the spatial affects caused by a curved or distorted plasma sheet in the simulation. For this study, we defined the center of the plasma sheet by using the position, where  $B_x$  passes through zero. We compared this surface with that of maximum thermal pressure, which gives a good approximation for the central plasma sheet (CPS) on the nightside [Ashour-Abdalla *et al.*, 2002], and found good agreement everywhere except  $x > -7.5$ , where the  $B_x$  surface organized the simulation results better. Figure 6 shows results from the simulation on the central plasma sheet before (Figure 6a) and during (Figure 6b) the

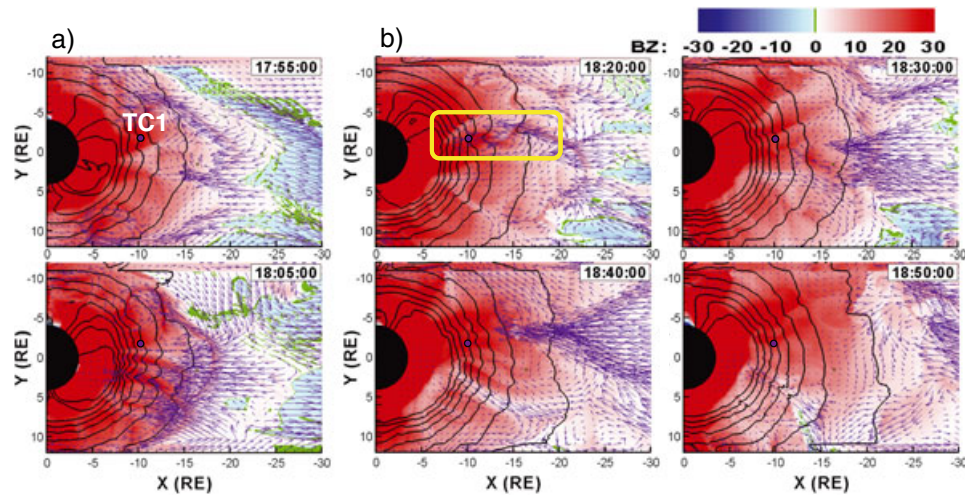


**Figure 6.** Simulation results in the central plasma sheet (a) before and (b) during the substorm. The background color shows  $B_z$  (–30–30 nT), the gray line contours show thermal pressure (0–4000 pPa,  $\delta P$  between contours is 500 pPa), and the purple arrows show the velocity in the  $xy$  plane. The purple dots indicate the location of TC1. The yellow box indicates an earthward propagating DF.

substorm. The background colors are  $B_z$ , the purple arrows are the velocity vectors, and the black contours are the thermal pressure between 0 and 4000 pPa,  $\delta P = 500$  pPa. The neutral line is where  $B_z$  is zero and is colored in green. The TC1 location is indicated by the purple dot in the images.

[16] A movie of CPS dynamics from the simulation is provided as supplementary information in the dynamic content for this paper. The movie frames use the same format as Figure 6. Table 1 contains an overview of timing of key events in the simulation along with satellite- and ground-based observations.

[17] The simulation results at the maximum pressure surface can be divided into distinct levels of activity during the

course of the event. Prior to 1655 UT,  $B_z$  is positive and there is very little activity in the CPS. During the interval 1655–1715 UT, the IMF is nearly eastward and there is some activity in the plasma sheet with a few DFs that originate at a distant neutral line and cease moving earthward at  $\sim -10 R_E$  except in the dusk sector near 2200 MLT where they reach  $\sim 7 R_E$  before being diverted. A strong tailward flow channel develops during this period that originates at  $\sim -10 R_E$  between 2200 and 2300 MLT at 1700 UT possibly due to ionospheric line-tying and steep pressure gradients in the region [Ashour-Abdalla et al., 2002; Walker et al., 2006]. A few minutes later strong earthward flows are also observed between 2200 and 2300 MLT, and a second tailward flow

**Table 1.** List of Times and Events in the Simulation Results and in Observations

Time (UT)	Simulation Events	Observations
1656–1715	Tailward flows begin to develop, Regions of minimum $B_z$ begin to develop near $\sim -10 R_E$ (1705 UT)	$AL$ fluctuates between $-50$ and $-220$ nT, PBI (1708–1710 UT), full auroral oval remains from a previous substorm in IMAGE auroral observations
1713–1750	Interval of moderate activity, patchy reconnection in the dusk sector near $x = -15 R_E$ generates DFs	$AL$ drops below $-200$ nT at 1713 UT and remains there until 1820 UT several PBIs and overall increase in auroral activity
1728–1745	Burst of several DFs travel earthward to $-8 R_E$	Interval of strong fluctuations in $AL$
1755–1815	The most active interval in the simulation (1755–1824 UT), reconnection regions merge to stretch across the entire tail, several DFs are generated and travel earthward, reconnection regions at $20-25 R_E$ in the tail	A second interval of strong oscillations in $AL$ , PBI in IMAGE observations (1757–1810 UT)
1817–1824	DF is generated at $\sim -18 R_E$ and travels earthward across the TC1 location at the end of the active interval	Pi2 onset at Urumqi at 1822 UT, auroral brightening observed near midnight by IMAGE
1825	Reconnection regions at $20-25 R_E$ weaken allowing fast flows from a reconnection region near $-35 R_E$ to enter the near-Earth region.	Auroral brightening near midnight intensifies but remains stationary
1827–1843	Final burst of DFs originating from $30$ to $35 R_E$ enter the near-Earth region in the midnight to dawn sector and strong tailward flows are observed in the dusk sector	Substorm onset at 1828 UT, poleward expansion of the auroral oval begins between 1827 and 1829 UT
1840–1847	Strong tailward flows divert earthward flows toward the dawn sector and velocities in the near-Earth region drop to low levels	$AL$ reaches a minimum at $\sim 1845$ UT and begins to recover at $\sim 1857$ UT

channel develops at  $\sim 0100$  MLT. A region of negative  $B_z$  develops between the two flow channels at  $\sim 1705$  UT and appears to be associated with reconnection on closed field lines. This process repeats itself with a third tailward flow channel developing at  $\sim 0200$  MLT and a new region of minimum  $B_z$  developing at  $\sim 1709$  UT. By  $\sim 1715$  UT, the minimum  $B_z$  regions have expanded to stretch between  $\sim -10$  and  $-20 R_E$  beginning a period of patchy reconnection. Between  $1715$  UT and  $\sim 1755$  UT, the patchy reconnection moves tailward to  $\sim -25 R_E$ .

[18] Beginning at  $1755$  UT, the neutral line stretches across the entire tail but stays fixed at  $\sim -25 R_E$  (Figure 6a). Several fast flows travel earthward from the neutral line but this time is not identified with substorm onset because the tail remains very active rather than going through the typical expansion and recovery phases. At  $\sim 1805$  UT, the neutral line breaks up and a second interval of patchy reconnection begins, centered between  $-25$  and  $-30 R_E$ . During this time, the magnetic field and pressure increase inside  $-15 R_E$  and the fast flows are slowed and diverted further back in the tail.

[19] There is another group of fast flows, originating from the reconnection regions at  $\sim -25 R_E$ , beginning at  $1816$  UT. The first, and strongest, DF of this group (indicated by the yellow box in Figure 6b) agrees most closely with the first DF observed by TC1 although the timing is off by  $\sim 5$  min. The DF penetrates in to  $\sim 8 R_E$  at  $1823$  UT at the time of the decrease in  $B_H$  observed at Norlisk and Pi2 onset observed at Urumqi and then continues earthward to reach  $\sim -6.5 R_E$  at  $1828$  UT. The Pi2 pulsations observed near the inner edge of the plasma sheet related to this DF are shown in Figure 4b and agree well with the TC1 Pi2 observations (Figure 4a), given a time shift of  $\sim 5$  minutes. The gray intervals in the plots indicated times when the Pi2 observed in the simulation correspond to the observations. At  $\sim 1825$  UT, some of the islands of reconnection weaken and we begin to see fast earthward flows from another reconnection region at  $\sim -30$  to  $-35 R_E$ . Based on both the simulation movie and the  $AL$  index (Figure 2), the period  $1715$ – $1828$  UT is a very disturbed period. There are some similarities with steady magnetospheric convection (SMC) events in that the thermal pressure and  $B_z$  build up in the inner magnetosphere causing the flows to be diverted further and further out in the tail over the course of the event [Kissinger *et al.*, 2012]. However, this event did not satisfy the definition of an SMC because the  $AL$  is not steady enough (J. Kissinger, personal communication, 2012).

[20] There is a final burst of DFs beginning at  $\sim 1830$  UT, in agreement with substorm onset in the  $AL$  index shown in Figure 2. A snapshot of the beginning of this burst of DFs is shown in Figure 6b. Initially, the flows penetrate to  $\sim -10 R_E$  but the pressure and magnetic field quickly build up causing the flows to be slowed and diverted further back in the tail. In the dusk sector ( $2200$ – $2300$  MLT) at  $\sim 1835$  UT, we see a tailward flow develop which disrupts the earthward flows. Between  $1830$  and  $1845$  UT, the increase in  $B_z$  and pressure resulting from the preceding burst of DFs cause the velocities in the region inside  $\sim -30 R_E$  to drop to very low values. After  $\sim 1850$  UT, the flows subside and the reconnection regions retreat tailward over most of the tail (see Figure 6b). There is a region of strong tailward flows after  $1850$  UT between  $2100$  and  $2200$  MLT. This may indicate the beginning of a steady magnetospheric convection

(SMC) period ( $1852$ – $2138$  UT) (J. Kissinger, personal communication, 2012).

[21] The timing of the sequence of events discussed above corresponds relatively well with the  $AL$  index (Figure 2) discussed in section 2. Bursts of DFs in the simulation occur at times indicated by the dashed blue lines in Figure 2 and correspond to periods of fluctuations in  $AL$ . During the interval  $1713$ – $1820$  UT, the  $AL$  index shows a moderate level of activity. This is reproduced in the simulation with the interval of patchy reconnection from a neutral line which stays relatively steady between  $-20$  and  $-25 R_E$ . There is a burst of DFs at approximately the correct time for substorm onset with a duration similar to that of the expansion phase ( $1830$ – $1845$  UT), and the activity in the plasma sheet subsides during the recovery phase in the  $AL$  index. There are several other DFs which propagate earthward as far as  $\sim -8 R_E$  throughout the simulation; however, only two of the DFs observed in the simulation are strong enough to disrupt the braking region boundary. The first nudges the boundary slightly at  $1806$  UT and corresponds to the first minimum in the  $AL$  index. The second, observed just before Pi2 and substorm onset, disrupts the boundary further, pushing it earthward to  $\sim -6.5 R_E$ .

[22] The sequence of events observed in the simulation also agrees well with the preonset auroral signatures discussed by Cao *et al.* [2012]. Fast earthward flows are observed in the simulation at  $1802$  and  $1820$  UT which are coincident with auroral streamers observed in the IMAGE data.

## 5. Analysis

[23] The first step to determine the relationship between the Pi2 pulsations and the DFs in the simulation is to identify the signatures of the two phenomena. By looking at the central plasma sheet in the simulation, we are able to identify DFs which appear as earthward/tailward propagating enhancements in  $B_z$  with  $\delta B_z \geq 6$  nT. Several DFs can be seen propagating earthward in the simulation after  $1700$  UT with the majority being confined within a few hours of local midnight. The DFs with the largest  $\delta B_z$  occur between  $2330$  and  $0115$  MLT. Figure 7a shows simulation results on the maximum pressure surface between  $1818$  and  $1823$  UT. The format is the same as Figure 6. The DF shown in these images is coincident with the TC1 observations and is confined to the region  $0015$ – $0115$  MLT. The large black arrows indicate the leading edge of the DF as it propagates earthward. Figure 7b shows the regions outlined by the yellow boxes at  $1821$  and  $1822$  UT. From these two images, one can see the obvious flow reversal on either side of the DF as well as a flow vortex that forms at the earthward edge of the structure [El-Alaoui, 2001; Ashour-Abdalla *et al.*, 2002; Walker *et al.*, 2006; El-Alaoui *et al.*, 2009; Ashour-Abdalla *et al.*, 2009; El-Alaoui *et al.*, 2010; Ge *et al.*, 2011; Birn *et al.*, 2011]. The center of the vortex, indicated by the yellow crosses, travels earthward  $\sim 1 R_E$  in the minute between the two time steps. Throughout the simulation interval, there are several BBFs that propagate with their associated DFs from reconnection regions between  $-12$  and  $-35 R_E$ . Each individual flow channel extends over many Earth radii in  $z$  but extends across only  $1$ – $3 R_E$  in  $y$  in GSM coordinates.



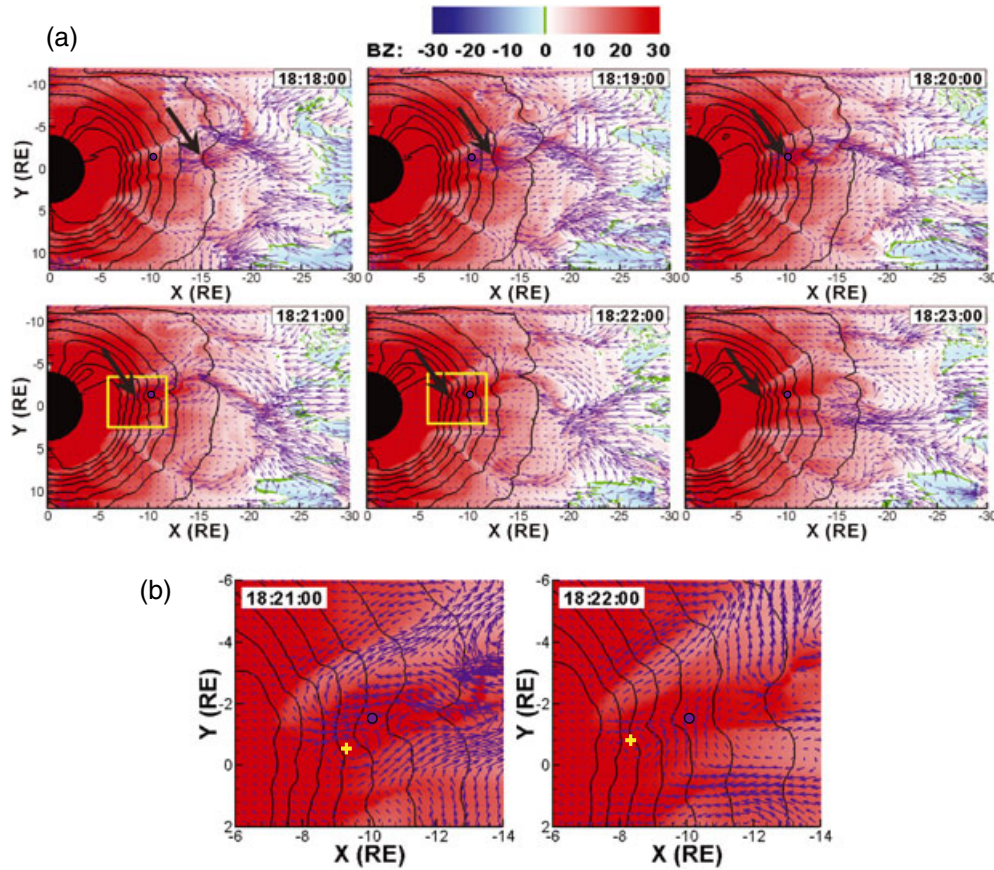


**Figure 7.** (a) Simulation results on the maximum pressure surface at 2 min intervals during the passage of a DF. The background color shows  $B_z$  (−30–30 nT), the gray line contours show thermal pressure (0–4000 pPa,  $\delta P$  between contours is 500 pPa), and the purple arrows show the velocity in the  $xy$  plane. The DF is indicated by the large blue arrow in each panel. The purple dots indicate the location of TC1. (b) The regions in the yellow boxes in the panels for 1821 and 1822 are expanded to show the flow vortex at the leading edge of the DF. Yellow crosses indicate the center of the vortex.

[24] The signatures associated with the DFs in the simulations are identified by averaging the simulated velocity, magnetic field, and pressure at fixed radial distances from 3 to 50  $R_E$  across a region of magnetic local time (MLT) where the dipolarization fronts are present. This allows us to see the effects that the DFs in a given local time range have on the inner magnetosphere as they travel earthward while averaging out the smaller scale spatial fluctuations within the DFs themselves. Next we take 10 min running averages and subtract them from the measured values to look only at the perturbations in the different components.

[25] As was stated before, most of the strongest DFs in the simulation are observed in the region 2330–0115 MLT; however, the strong DF observed at onset is located in the region 0015–0115 MLT. Figures 8a and 8b show the central plasma sheet at 1820 UT in the same format as the panels in Figure 6. The gray lines in Figure 8a indicate 2330 and 0115 MLT, and the black lines in Figure 8b indicate 0015 and 0115 MLT. Figure 8c shows the perturbations on the central plasma sheet in the average of  $B_z$  between 2330 and 0115 MLT, and Figure 8d shows the perturbations in  $B_z$  between 0015 and 0115 MLT, plotted versus time and

radial distance from Earth in  $R_E$ . The earthward propagating DFs can be seen in  $B_z$  (Figures 8c and 8d) as sharp boundaries between negative (blue) and positive (red) contours. The paths of the strongest, most coherent DFs identified in Figures 8c and 8d have been traced (dashed black lines). The line plots at Figures 8c and 8d (bottom) show  $\delta B_z$  at  $r = -6, -8, -10$ , and  $-12 R_E$  filtered to Pi2 frequencies using a band-pass filter. The blue arrows on the line plots indicate the times when DFs were observed at the given radial distance in the tail. The solid purple lines indicate Pi2 onset at Urumqi (1822 UT) and substorm onset identified in  $AL$  (1828 UT). Gray-highlighted intervals in Figure 8d are times when Pi2 frequency oscillations are found at and immediately after the dipolarization front observed at onset. In Figure 8d, there are bursts of fluctuations within the Pi2 range following each of the DF observed at onset (highlighted in gray). Additional Pi2 period perturbations prior to onset and related to DFs outside of the MLT region selected are indicated by dashed boxes.

[26] In order to focus on the perturbations related to the DF observed by TC1 at onset, we focus on the region between 0015 and 0115 MLT. In addition, since TC1 was near the edge of the plasma sheet during the time leading up

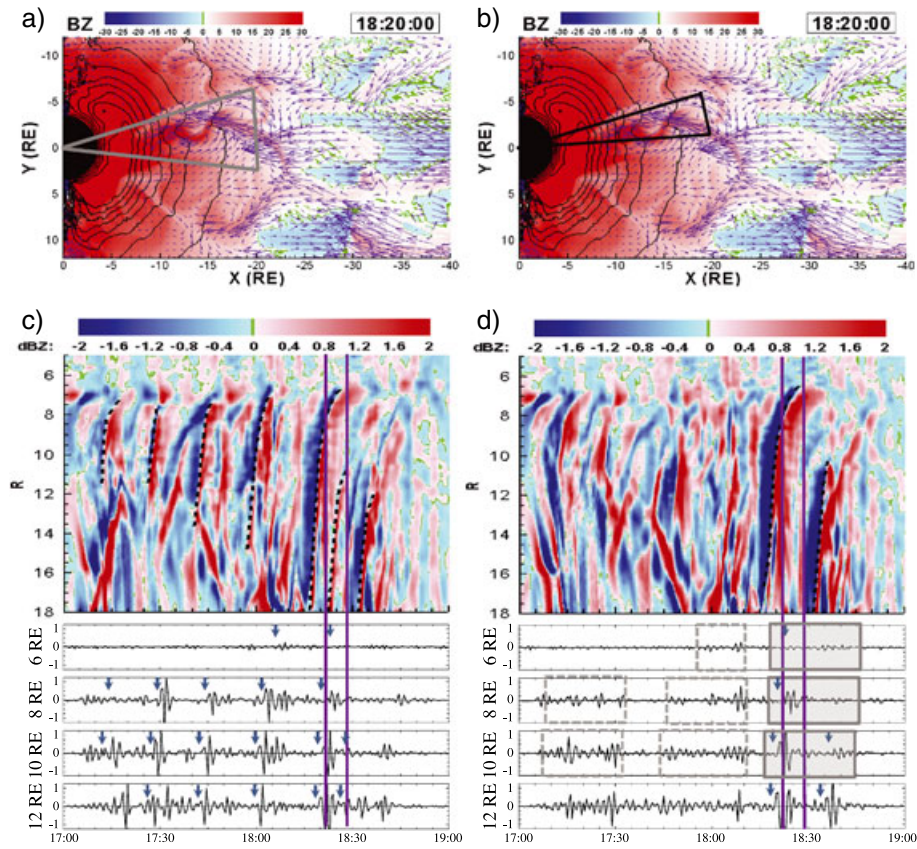


**Figure 8.** (a) An image of the simulated CPS at 1820 UT in the same format as Figure 6 with the region 2330–0115 MLT indicated by the gray lines. (b) Same as Figure 8a but with the region 0015–0115 MLT indicated by the black lines. (c) Perturbed variables in  $B_z$  on the CPS averaged over the region 2330–0115 MLT plotted versus time in  $x$  and radial distance from Earth in  $y$ . The dashed lines identify the paths of strong DFs. (bottom) Line plots of the perturbed variables at  $r = 6, 8, 10$ , and  $12 R_E$ . Vertical lines indicate Pi2 and substorm onset. Blue arrows identify the passage of strong DFs. (d) Same as Figure 8c for the region 0015–0115 MLT. Gray-highlighted intervals are times when the frequencies of the oscillations related to the DF at onset are within the Pi2 range. Dashed boxes indicate Pi2 fluctuations related to DFs outside the selected local time region.

to onset, we focus on the surface  $1.5 R_E$  above the minimum  $B_x$  plane. Figure 9a shows the perturbations in the radial component of the magnetic field on a plane  $1.5 R_E$  above the minimum  $B_x$  plane. Ground-based observations, filtered to a 30 s time step to match the simulation results, are shown at the bottom of the figure for comparison. The dashed black lines have been copied from Figure 8d to show how the perturbations relate to the path of the DFs. Pi2 fluctuations are observed at  $-6 R_E$ , highlighted in gray in the line plots, as the DF at onset approaches and begins to disrupt the braking region. The onset of these perturbations is at 1819 UT, a few minutes before Pi2 onset on the ground, and the fluctuations continue for about 30 min which agrees well with the duration of Pi2 in the Urumqi observations. Fluctuations are also evident in the radial component of the magnetic field at  $-6 R_E$ , during the SMC-like interval, that are related to DFs just outside the selected MLT range (dashed gray boxes in Figure 9a). The  $B_R$  component is interesting because it shows the fluctuations that are propagating across the magnetic field lines. These are the fluctuations that would be observed at middle to low latitudes.

[27] Figure 9b shows that the fluctuations in  $\delta P_{\text{total}}$  (thermal pressure plus magnetic pressure) on a plane  $1.5 R_E$  above the minimum  $B_x$  plane are also coincident with the passage of DFs through the region. Following the DF at onset, there are fluctuations in the line plots from  $-12$  to  $-6 R_E$  with a period of  $\sim 120$ – $150$  s (highlighted in gray).

[28] Figure 10 shows line plots of the perturbations in the magnetic pressure (red), thermal pressure (green), and total pressure (black) at the minimum  $B_x$  plane and  $1.5 R_E$  above the plane at  $-6$  (Figures 10a and 10b),  $-8$  (Figures 10c and 10d), and  $-10$  (Figures 10e and 10f)  $R_E$  in the magnetotail from 1745 to 1845 UT. The blue vertical lines indicate the time the DF reached the given radial distance, and the dashed black lines indicate Pi2 and substorm onset. In general, the fluctuations in the magnetic and total pressures  $1.5 R_E$  above minimum  $B_x$  surface, near the edge of the plasma sheet, are out of phase. On the minimum  $B_x$  surface, fluctuations are more often in phase suggesting a fast-mode wave. The perturbations at the time of the DF crossing are typically in antiphase suggesting a slow-mode wave. The exception is at  $-6 R_E$  on the minimum  $B_x$  surface where the



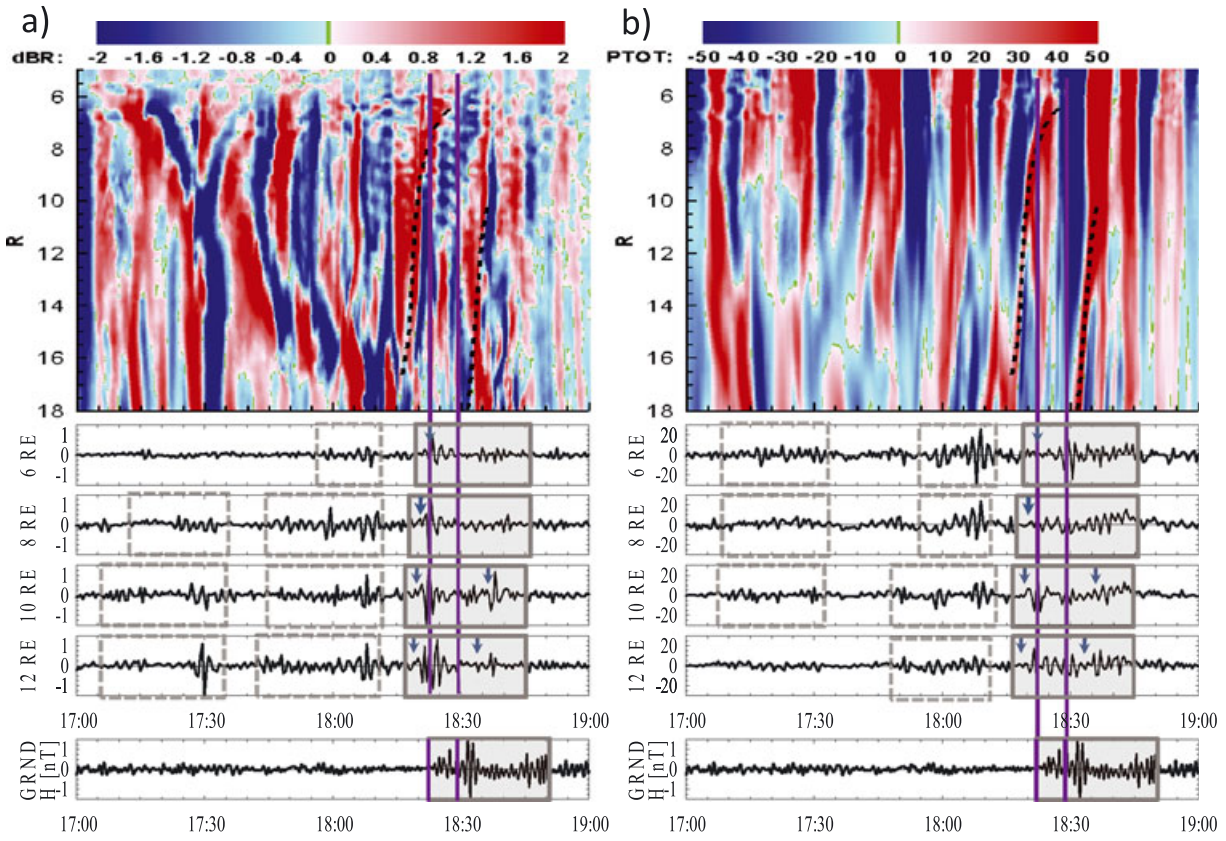


**Figure 9.** Perturbed variables (a)  $\delta B_R$  and (b) the perturbed total pressure  $\delta P_{\text{total}}$  plotted in the same format as Figure 8d. Ground magnetometer observations filtered to 30 s resolution have been included at the bottom of the figure for comparison.

perturbations are in phase at the time of the DF. In the center of the plasma sheet at  $-10 R_E$  (Figure 10e), the total and magnetic pressures are only in phase for a short time beginning at 1821 UT, just before Pi2 onset. Near the edge of the plasma sheet at  $-10 R_E$  (Figure 10f), the fluctuations in the magnetic pressure in Figure 10d very closely resemble the Pi2 observed by TC1 beginning at 1822 UT (see Figure 4a).

[29] Figure 11 shows the perturbations in (Figure 11a) the velocity parallel to the magnetic field ( $\delta v_{\text{pa}}$ ), and (Figure 11b) the velocity in the earthward direction ( $\delta v_x$ )  $1.5 R_E$  above the plasma sheet plotted in the same format as Figure 8. The amplitude of the fluctuations observed in  $\delta v_{\text{pa}}$  (Figure 11a) generally increase following the passage of a DF, and perturbations are observed in to  $-6 R_E$  following the DF at onset. Pi2 period fluctuations related to DFs outside the selected MLT region are observed at 1705–1730 UT and 1745–1810 UT (dashed gray boxes). The first of these intervals is associated with a strong minimum in  $B_z$  at the beginning of the disturbed period in the simulation. The second interval occurs just before the first minimum in the  $AL$  index discussed above. The interval related to the DF at onset (highlighted in gray) occurs just before and during the expansion phase of the substorm and may represent the precursor to the Pi2 observed on the ground at Urumqi. The enhancement in  $\delta v_{\text{pa}}$  tailward of the braking region, along the path of the DF within the Pi2 range may be associated with TR Pi2.

[30] The amplitude of the fluctuations in  $\delta v_x$  (Figure 11b) increase slightly before the DFs passage through the region.

However, we must remember that the fluctuations are over a range in MLT from 0015 to 0115 UT. Because the flow channels are so narrow ( $1-2 R_E$ ) (see Figure 7), Figure 11a shows the effects of the interaction between several

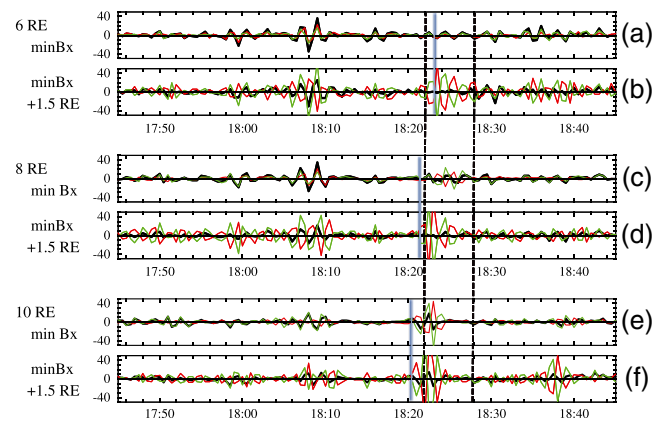


**Figure 10.** Perturbations in the thermal pressure (green), magnetic pressure (red), and total pressure (black) (pPa) at  $-6$ ,  $-8$ , and  $-10 R_E$  between 0015 and 0115 MLT. For each radial distance, perturbations are shown on the minimum  $B_x$  surface, and  $1.5 R_E$  above the minimum  $B_x$  surface. Blue vertical lines indicate the times the DFs were observed at the given radial distances, and the dashed black lines indicate Pi2 and substorm onset.

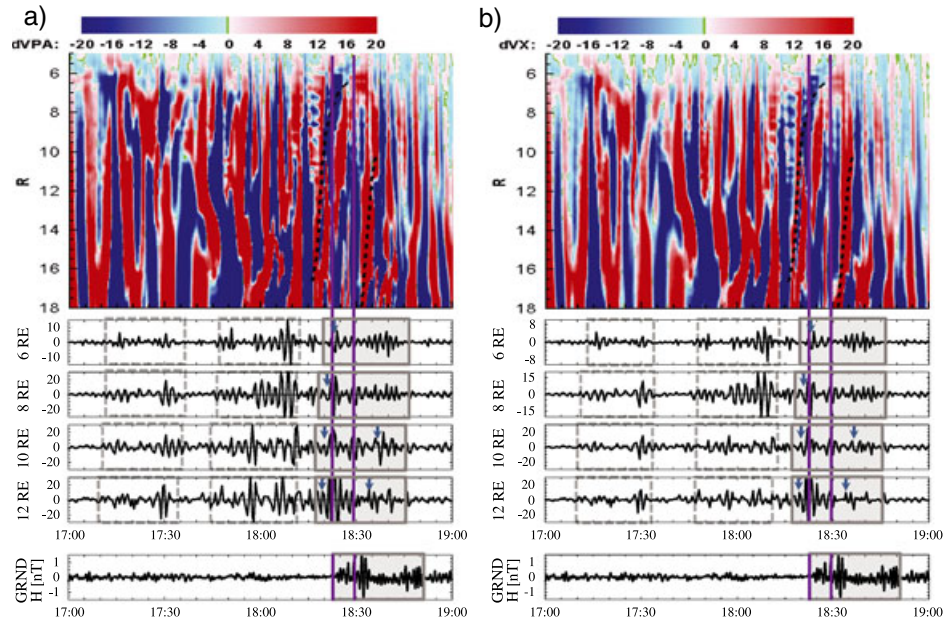


**Figure 11.** Perturbed variables (a)  $\delta v_{||}$  and (b)  $\delta v_x$  plotted in the same format as Figure 9.

earthward flow channels and rebound flows located outside of the MLT region. Fluctuations in  $\delta v_x$  are well correlated with fluctuations in  $\delta B_R$ . The line plots at the bottom of Figure 11b show that the amplitude of the fluctuations in  $\delta v_x$  decreases by more than 50% as the disturbances move earthward from  $-12$  to  $-8 R_E$ . The fluctuations in  $\delta v_x$  associated with the DF at onset agree very well with the duration of the Pi2 observed on the ground, and the fluctuations earlier in the simulation agree well with the timing of the first drop and the first minimum in the  $AL$  index (Figure 2).

## 6. Discussion

[31] Previous studies have used satellite measurements to investigate the origin of Pi2 pulsations and build models to describe how they are generated. The benefits of using a global MHD simulation to investigate the relationship between the DFs and the Pi2 pulsations is that we can examine the entire region where the bursty flows, DFs and Pi2 pulsations are present rather than using data from single points in space. This allows us to identify possible source regions and to track the evolution of the pulsations as they move through the simulation.

[32] In order for the pulsations observed at  $-6 R_E$  to propagate earthward to drive the Pi2 at lower L shells, the azimuthal scale size must be large. Using the simulation results, we have taken several MLT bins and examined the coherence between them. Figure 12 shows the perturbations in  $B_T$  in 15 min MLT bins between 2330 and 0145 MLT on the surface  $1.5 R_E$  above the center of the plasma sheet for the interval 1730–1900 UT. The panels show the MLT bins (Figure 12a) 2330–2345, (Figure 12b) 2345–0000, (Figure 12c) 0000–0015, (Figure 12d) 0015–0030, (Figure 12e) 0030–0045, (Figure 12f) 0045–0100, (Figure 12g) 0100–0115, (Figure 12h) 0115–0130, and (Figure 12i) 0130–0145 MLT. The values for coherence between the bin 0030–0045 MLT and the other MLT bins

for the shaded intervals (1805–1813 UT and 1819–1829 UT) range from 0.6 to 0.85 for the low end of the Pi2 spectrum (6–11 mHz). In general, the magnetic field perturbations during the shaded intervals on this surface show good coherence over  $\sim 1.5$  to 2 h MLT. This is consistent with a recent study by Kwon *et al.* [2012] which show high coherence if the signals (multiple satellites and ground-based observations) are within 3 h MLT of each other. However, although we see coherence across several MLT bins above the center of the plasma sheet during the expansion phase of the substorm (1819–1829 UT), and the waveforms at  $-6 R_E$  in the simulated magnetic pressure look very much like the observations, we only see coherence across  $\sim 1$  h of MLT near the center of the plasma sheet. Therefore, it is difficult to determine a direct causal relationship between the pulsations we observe in the simulation and the midlatitude observations by Urumqi magnetometer, and higher latitude Pi2 observations are unavailable for this event. We can, however, use the ground observations for a timing comparison with the simulation.

[33] Based on Figures 8, 9, and 11, the simulation shows Pi2 period pulsations at  $-6 R_E$  prior to  $\sim 1823$  UT. This is in contrast to the observations which only show Pi2 pulsations after 1823 UT. There is a short ( $\sim 10$  min) burst of weak Pi2 pulsations just after 1730 UT in the observations that may be related to the earlier DFs observed in the simulation and the first drop in  $AL$ , but there is nothing in the observations that could correspond to the fluctuations between 1755 and 1805 UT in the simulation. One reason for the discrepancy may be that the DFs were in the wrong local time for the Pi2 to be observed by the Urumqi station. This may be especially true for the DF burst at 1755–1805 UT which was predominantly on the duskside while Urumqi was on the dawnside at  $\sim 0200$  MLT. Another possibility is that the fluctuations observed at  $-6 R_E$  in the simulation prior to onset are not able to propagate earthward to be observed at lower latitudes. Due to the lack of an inner magnetosphere/plasmasphere model in the



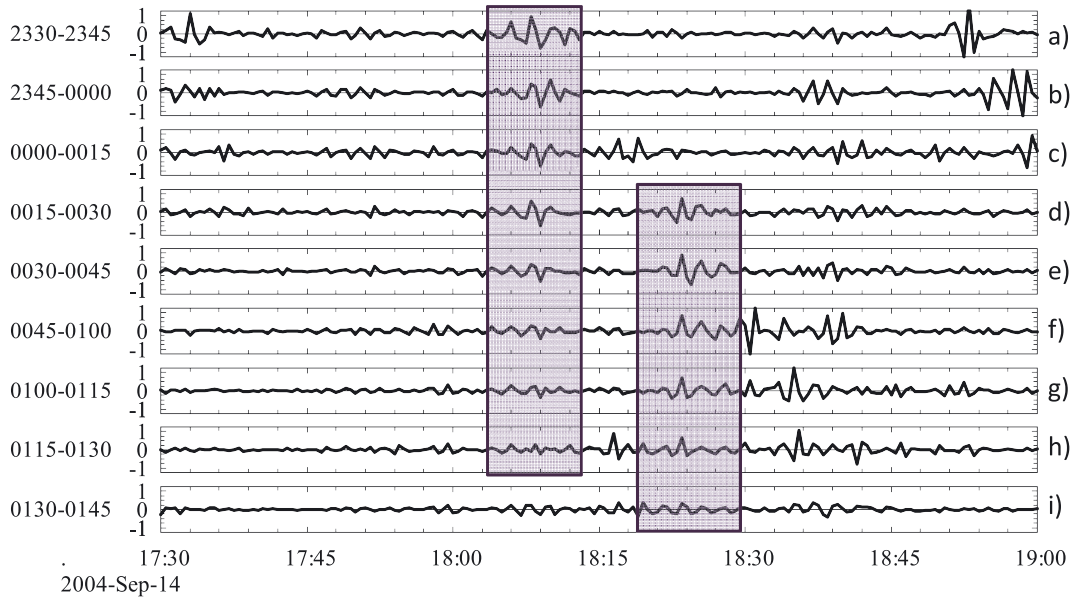


**Figure 12.** Perturbations in  $B_T$  at  $-6 R_E$  and  $1.5 R_E$  above the plasma sheet in the MLT bins (a) 2330–2345, (b) 2345–0000, (c) 0000–0015, (d) 0015–0030, (e) 0030–0045, (f) 0045–0100, (g) 0100–0115, (h) 0115–0130, and (i) 0130–0145 MLT. The shading indicates MLT bins which have good coherence to the bin at 0030–0045 MLT in the perturbations related to the DFs observed during the first minimum in  $AL$  (1085–1813 UT) and at onset (1819–1929 UT).

MHD simulation, we are not able to investigate the propagation of Pi2 to lower latitudes and we leave this topic for future research.

[34] Focusing on the perturbations at substorm onset, Figure 9b shows that perturbations with Pi2 periods are present in the  $\delta P_{\text{total}}$  from  $-6$  to  $-14 R_E$  between  $\sim 1815$  and  $1845$  UT, when the burst of DFs was observed near the time of onset. During this interval, the simulation shows at least six individual DFs of varied intensities which form and travel earthward within a time span of  $\sim 30$  min at locations between  $\sim 2230$  and  $0130$  MLT. The pressure fluctuations may be initiated by the passage of the strong DF and then amplified by the succeeding DFs. The fluctuations in pressure can also be identified in Figure 7 as the perturbations in the thermal pressure contours (gray contours) surrounding the flow channel as the DF travels earthward. There is also a tailward displacement of the pressure contours associated with the tailward flows on either side of the flow channel. Each time a new DF enters the region, a new indentation in the pressure contours forms and migrates toward either flank. During active periods in the simulation, several of these indentations can be observed on each of the pressure contours. The perturbations in the pressure near the center of the plasma sheet (see Figures 10a, 10c, and 10e) following the arrival of the DFs may be related to the fast-mode wave which propagates into the inner magnetosphere to generate low-latitude to midlatitude Pi2. We also observe earthward velocity perturbations all the way in to  $-6 R_E$  (Figure 11b) that are related to the fluctuations in the pressure which agrees well with the directly driven category of Pi2 [Kepko *et al.*, 2001].

[35] Each time a bursty flow and its associated DF travel earthward in the simulation, the flows at the earthward edge

of the DF are diverted to either side of the flow channel. As the flows are diverted, they interact with the background flows and neighboring flow channels which cause further diversion. In many cases, the flows eventually turn tailward. The tailward flows then interact with subsequent earthward flows to create flow perturbations and vortices. The resulting vortices can be seen in the velocity vectors in Figure 7b. As the DFs reach the inner magnetosphere, we begin to see tailward flows to either side of the initial earthward flow channel. The interactions become more pronounced during the intervals of intense activity due to the fact that there are several DFs which travel earthward in a short amount of time during this period. Velocity fluctuations intensify each time a new DF passes through the region (highlighted in gray) indicating that the DFs may act to enhance the existing perturbations bringing them above the ambient noise levels in the region (see Figure 11). There are also velocity perturbations associated with DFs outside the selected MLT region (dashed gray boxes in Figure 11) which result from the interactions between the various flow channels. As discussed in the previous section, each of the intervals corresponds to a period when there are large fluctuations in the  $AL$  index (see Figure 2).

[36] In Figure 8c, there is a steady boundary in the field at  $-7.5 R_E$  until  $1805$  UT when a DF enters the region and causes the boundary to distort slightly. Before the braking region has time to recover, another strong DF penetrates to  $\sim -6.5 R_E$  at  $1823$  UT and distorts the braking region further. Only after the braking region is distorted do we have Pi2 period fluctuations in  $\delta B_z$  inside  $-7 R_E$ . The timing and duration of the interval when Pi2 period perturbations in  $\delta B_z$  are observed inside  $-7 R_E$  ( $1830$ – $1845$  UT), associated with the DF at  $1815$ – $1824$  UT in the simulation, agrees well with

expansion phase of the substorm and with the duration of the second packet of Pi2 (1840–1855 UT) in the ground-based observations. In addition, the perturbations in  $v_{pa}$  associated with the DFs at 1830 to 1855 UT are observed at  $-6 R_E$  and may be related to the inertial current (IC) Pi2s described by *Kepko et al.* [2001]. IC Pi2 appears to be generated by the vortices formed through interactions between the flows and rebound flows associated with the successive DFs as they enter the near-Earth region. However, the velocity perturbations are quickly damped earthward of  $\sim -7 R_E$  except for during the intervals when a strong DF has disrupted the steep pressure and magnetic field gradients in the braking region.

## 7. Summary

[37] In order to better understand generation of Pi2 and how they are associated with substorm dynamics, we need a global view of the magnetosphere. We have investigated the generation of Pi2 waves in the tail by DFs propagating earthward from a near-Earth neutral line by analyzing a global MHD simulation of a substorm event on 14 September 2004. Because global MHD simulations provide estimates of the critical parameters throughout the inner magnetosphere, they are valuable tools for studying such processes as the generation of Pi2 and determining how they link to earthward propagating dipolarization fronts. The sequence of events in the simulations is similar to that inferred from observations by the Double Star, and IMAGE spacecraft, and the variations of the *AL* index, indicating that the simulation has done a reasonable job of reproducing the state of the magnetotail for this event. The substorm begins at  $\sim 1828$  UT and is preceded by an interval of enhanced but variable convection. Both the initial period and the substorm have multiple DFs which lead to vorticity. The DFs observed in the simulation are very localized with an azimuthal extent on the order of  $1\text{--}2 R_E$ . Several dipolarization fronts have been identified in the simulation and are linked to Pi2 frequency fluctuations in the magnetic field, velocity, and pressure inside  $-13 R_E$ , but not all of the flows make it into the inner magnetosphere to generate Pi2 pulsations inside the braking region.

[38] Considering the Pi2 period fluctuations outside the braking region, there is good agreement between observations by TC1 and fluctuations in the simulation at a location similar to that of TC1. We cannot draw a direct relationship between the Urumqi observations and the pulsations inside the braking region in the simulation since the pulsations near the plasma sheet are only coherent over about 1 h of MLT. However, we have shown good agreement in the relative timing of the Pi2 pulsations when comparing the observations and the simulation. The timing and location of dipolarization fronts and Pi2 pulsations in the simulation lead us to believe that the Pi2 waves are generated by the DFs in agreement with several models developed to explain observations [e.g., *Kepko et al.*, 2001, 2004].

[39] Our main conclusions can be summarized as follows: (1) Dipolarization fronts create perturbations in  $B_z$  which have periods in the Pi2 range, but the perturbations quickly damp unless there are subsequent DFs to keep the oscillations going. (2) There are Pi2 period perturbations in the total pressure, and  $B_R$  at  $\sim -6$  to  $-12 R_E$  following the DFs observed at onset. The Pi2 period pulsations in both total

pressure and  $B_R$  at  $-6 R_E$  beginning shortly before Pi2 onset in the observations agree well with ground-based observations. (3) Pulsations with periods within the Pi2 range are observed in the velocity components inside  $\sim -13 R_E$  throughout the simulation and are enhanced directly following the passage of each flow burst observed when we look at the region 0015–0115 MLT. It appears that the compression and rebound of the BBFs and their associated DFs as they approach the braking region produce the Pi2 signatures in agreement with *Kepko et al.* [2001]. (4) The DFs in the simulation between 1715 and 1820 UT all stop tailward of  $-7.5 R_E$  without causing serious disruption to the braking region, and the magnetic field perturbations associated with them are quickly damped. The fluctuations inside the braking region appear to be driven by perturbations in total pressure,  $B_R$ ,  $v_{pa}$ , and  $v_x$  associated with the BBFs even though the  $B_z$  signatures dissipate tailward of the braking region.

[40] **Acknowledgments.** This research was support by the NASA Graduate Student Research Program through Goddard Space Flight Center, grant NNX10AM08H. This research was also supported at UCLA and the Goddard Space Flight Center by an Interdisciplinary Science grant from the Magnetospheric Multiscale project (NASA grant NNX08AO48G at UCLA). M. El-Alaoui was supported by NASA grant NNX10AQ47G. Computational resources were provided by the Extreme Science and Engineering Discovery Environment (XSEDE), which is supported by National Science Foundation grant OCI-1053575. R.J. Walker's contribution to this work was supported as Individual Research and Development while he was at the National Science Foundation. M.G. Kivelson was supported by NASA grant UCB/NASA NAS 5-02099. We acknowledge the experiment teams that acquired, processed, and provided the OMNI-included data, and J.H. King and N.E. Papitashvili of NASA/GSFC for creating the OMNI data set. Geotail magnetic field data were provided by T. Nagai, JAXA in Japan. Geotail and OMNI data were obtained through the Virtual Magnetospheric Observatory (VMO). We acknowledge C. Carr and the Double Star TC1 FGM instrument team, as well as ESA, Double Star, Center for Space Science and Applied Research, and the Chinese Academy of Sciences for Double Star data. We also acknowledge the World Data Center for Geomagnetism, Kyoto, and the Geomagnetic Network of China, for Pi2 and geomagnetic field data, and the SuperMAG network for Norilsk magnetometer data. We would also like to thank Krishan Khurana, Tung-Shin Hsu, and Robert J. Strangeway for helpful discussions concerning this research.

[41] Robert Lysak thanks Kazue Takahashi and two anonymous reviewers for their assistance in evaluating this paper.

## References

- Angelopoulos, V., W. Baumjohann, C. F. Kennel, F. V. Coroniti, M. G. Kivelson, R. Pellat, R. J. Walker, H. Luehr, and G. Paschmann (1992), Bursty bulk flows in the inner central plasma sheet, *J. Geophys. Res.*, **97**, 4027–4039, doi:10.1029/91JA02701.
- Angelopoulos, V., C. F. Kennel, F. V. Coroniti, R. Pellat, M. G. Kivelson, R. J. Walker, C. T. Russell, W. Baumjohann, W. C. Feldman, and J. T. Gosling (1994), Statistical characteristics of bursty bulk flow events, *J. Geophys. Res.*, **99**, 21,257–21,280, doi:10.1029/94JA01263.
- Angelopoulos, V., et al. (2008), Tail reconnection triggering substorm onset, *Science*, **321**, 931–935, doi:10.1126/science.1160495.
- Ashour-Abdalla, M., M. El-Alaoui, F. V. Coroniti, R. J. Walker, and V. Peromian (2002), A new convection state at substorm onset: Results from an MHD study, *Geophys. Res. Lett.*, **29**(20), 1965, doi:10.1029/2002GL015787.
- Ashour-Abdalla, M., J.-M. Bosqued, M. El-Alaoui, V. Peromian, M. Zhou, R. Richard, R. Walker, A. Runov, and V. Angelopoulos (2009), A simulation study of particle energization observed by THEMIS spacecraft during a substorm, *J. Geophys. Res.*, **114**, A09204, doi:10.1029/2009JA014126.
- Ashour-Abdalla, M., M. El-Alaoui, M. L. Goldstein, M. Zhou, D. Schriver, R. Richard, R. Walker, M. G. Kivelson, and K.-J. Hwang (2011), Observations and simulations of non-local acceleration of electrons in magnetotail magnetic reconnection events, *Nat. Phys.*, **7**, 360–365, doi:10.1038/nphys1903.
- Birn, J., R. Nakamura, E. V. Panov, and M. Hesse (2011), Bursty bulk flows and dipolarization in MHD simulations of magnetotail reconnection, *J. Geophys. Res.*, **116**, A01210, doi:10.1029/2010JA016083.

- Cao, X., et al. (2008), Multispacecraft and ground-based observations of substorm timing and activations: Two case studies, *J. Geophys. Res.*, **113**, A07S25, doi:10.1029/2007JA012761.
- Cao, X., et al. (2012), Auroral streamers implication for the substorm progression on September 14, 2004, *Planet. Space Sci.*, **71**, 119–124, doi:10.1016/j.pss.2012.07.018.
- Carr, C., et al. (2005), The double Star magnetic field investigation: Instrument design, performance and highlights of the first year's observations, *Ann. Geophys.*, **23**, 2713–2732, doi:10.5194/angeo-23-2713-2005.
- Chang, R. P. H., and L. J. Lanzerotti (1975), On the generation of magnetohydrodynamic waves at the onset of a substorm, *Geophys. Res. Lett.*, **2**, 489–491, doi:10.1029/GL002i011p00489.
- Chen, C. X., and R. A. Wolf (1993), Interpretation of high-speed flows in the plasma sheet, *J. Geophys. Res.*, **98**, 21,409–21,419, doi:10.1029/93JA02080.
- Chen, C. X., and R. A. Wolf (1999), Theory of thin-filament motion in Earth's magnetotail and its application to bursty bulk flows, *J. Geophys. Res.*, **104**, 14,613–14,626, doi:10.1029/1999JA900005.
- Davis, T. N., and M. Sugiura (1966), Auroral electrojet activity index AE and its universal time variations, *J. Geophys. Res.*, **71**, 785–801, doi:10.1029/JZ071i003p00785.
- El-Alaoui, M. (2001), Current disruption during November 24, 1996 substorm, *J. Geophys. Res.*, **106**, 6229–6246, doi:10.1029/1999JA000260.
- El-Alaoui, M., M. Ashour-Abdalla, R. J. Walker, V. Peromian, R. L. Richard, V. Angelopoulos, and A. Runov (2009), Substorm evolution as revealed by THEMIS satellites and a global MHD simulation, *J. Geophys. Res.*, **114**, A08221, doi:10.1029/2009JA014133.
- El-Alaoui, M., M. Ashour-Abdalla, R. L. Richard, M. L. Goldstein, J. M. Weygand, and R. J. Walker (2010), Global magnetohydrodynamic simulation of reconnection and turbulence in the plasma sheet, *J. Geophys. Res.*, **115**, A12236, doi:10.1029/2010JA015653.
- Frank, L. A., K. L. Ackerson, W. R. Paterson, J. A. Lee, M. R. English, and G. L. Pickett (1994), The comprehensive plasma instrumentation (CPI) for the geotail spacecraft, *J. Geomagn. Geoelec.*, **46**, 23–37.
- Gabrielese, C., et al. (2009), Timing and localization of near-Earth tail and ionospheric signatures during a substorm onset, *J. Geophys. Res.*, **114**, A00C13, doi:10.1029/2008JA013583.
- Ge, Y. S., J. Raeder, V. Angelopoulos, M. L. Gilson, and A. Runov (2011), Interaction of dipolarization fronts within multiple bursty bulk flows in global MHD simulations of a substorm on 27 February 2009, *J. Geophys. Res.*, **116**, A00123, doi:10.1029/2010JA015758.
- Gjerloev, J. W. (2009), A global ground-based magnetometer initiative, *EOS Trans.*, **90**, 230–231, doi:10.1029/2009EO270002.
- Gjerloev, J. W. (2012), The SuperMAG data processing technique, *J. Geophys. Res.*, **117**, A09213, doi:10.1029/2012JA017683.
- Hesse, M., and J. Birn (1991), On dipolarization and its relation to the substorm current wedge, *J. Geophys. Res.*, **96**, 19,417–19,426, doi:10.1029/91JA01953.
- Hones, E. W. Jr., T. Pytte, and H. I. Jr. West (1984), Associations of geomagnetic activity with plasma sheet thinning and expansion—A statistical study, *J. Geophys. Res.*, **89**, 5471–5478, doi:10.1029/JA089iA07p05471.
- Hsu, T.-S., and R. L. McPherron (2007), A statistical study of the relation of Pi 2 and plasma flows in the tail, *J. Geophys. Res.*, **112**, A05209, doi:10.1029/2006JA011782.
- Hsu, T.-S., R. L. McPherron, V. Angelopoulos, Y. Ge, H. Zhang, C. Russell, X. Chu, and J. Kissinger (2012), A statistical analysis of the association between fast plasma flows and Pi2 pulsations, *J. Geophys. Res.*, **117**, A11221, doi:10.1029/2012JA018173.
- Keiling, A., et al. (2008), Correlation of substorm injections, auroral modulations, and ground Pi2, *Geophys. Res. Lett.*, **35**, L17S22, doi:10.1029/2008GL033969.
- Keiling, A., and K. Takahashi (2011), Review of Pi2 models, *Space Sci. Rev.*, **161**, 63–148, doi:10.1007/s11214-011-9818-4.
- Kepko, L., and M. Kivelson (1999), Generation of Pi2 pulsations by bursty bulk flows, *J. Geophys. Res.*, **104**, 25,021–25,034, doi:10.1029/1999JA900361.
- Kepko, L., M. G. Kivelson, and K. Yumoto (2001), Flow bursts, braking, and Pi2 pulsations, *J. Geophys. Res.*, **106**, 1903–1916, doi:10.1029/2000JA000158.
- Kepko, L., M. G. Kivelson, R. L. McPherron, and H. E. Spence (2004), Relative timing of substorm onset phenomena, *J. Geophys. Res.*, **109**, A04203, doi:10.1029/2003JA010285.
- Kim, K.-H., K. Takahashi, S. Ohtani, and S.-K. Sung (2007), Statistical analysis of the relationship between earthward flow bursts in the magnetotail and low-latitude Pi2 pulsations, *J. Geophys. Res.*, **112**, A10211, doi:10.1029/2007JA012521.
- Kissinger, J., R. L. McPherron, T.-S. Hsu, and V. Angelopoulos (2012), Diversion of plasma due to high pressure in the inner magnetosphere during steady magnetospheric convection, *J. Geophys. Res.*, **117**, A05206, doi:10.1029/2012JA017579.
- Kokubun, S., T. Yamamoto, M. H. Acuna, K. Hayashi, K. Shiokawa, and H. Kawano (1994), The geotail magnetic field experiment, *J. Geomagn. Geoelec.*, **46**, 7–21.
- Kwon, H.-J., et al. (2012), Local time-dependent Pi2 frequencies confirmed by simultaneous observations from THEMIS probes in the inner magnetosphere and at low-latitude ground stations, *J. Geophys. Res.*, **117**, A01206, doi:10.1029/2011JA016815.
- McPherron, R. L. (1972), Substorm related changes in the geomagnetic tail: The growth phase, *Planet. Space Sci.*, **20**(9), 1521–1539, doi:10.1016/0032-0633(72)90054-2.
- Mende, S. B., H. U. Frey, M. Lampton, J.-C. Gerard, B. Hubert, S. Fuselier, J. Spann, R. Gladstone, and J. L. Burch (2001), Global observations of proton and electron auroras in a substorm, *Geophys. Res. Lett.*, **28**, 1139–1142, doi:10.1029/2000GL012340.
- Miyashita, Y., S. Machida, T. Mukai, Y. Saito, K. Tsuruda, H. Hayakawa, and P. R. Sutcliffe (2000), A statistical study of variations in the near and midtail magnetotail associated with substorm onsets: Geotail observations, *J. Geophys. Res.*, **105**, 15,913–15,930, doi:10.1029/1999JA000392.
- Miyashita, Y., et al. (2009), A state-of-the-art picture of substorm-associated evolution of the near-Earth magnetotail obtained from superposed epoch analysis, *J. Geophys. Res.*, **114**, A01211, doi:10.1029/2008JA013225.
- Murphy, K. R., I. J. Rae, I. R. Mann, A. P. Walsh, D. K. Milling, and A. Kale (2011), The dependence of Pi2 waveforms on periodic velocity enhancements within bursty bulk flows, *Ann. Geophys.*, **29**, 493–509, doi:10.5194/angeo-29-493-2011.
- Nagai, T., M. Fujimoto, R. Nakamura, Y. Saito, T. Mukai, T. Yamamoto, A. Nishida, S. Kokubun, G. D. Reeves, and R. P. Lepping (1998), Geotail observations of a fast tailward flow at  $X_{GSM} = -15R_E$ , *J. Geophys. Res.*, **103**, 23,543–23,550, doi:10.1029/98JA02246.
- Nakamura, R., et al. (2005), Cluster and Double Star observations of dipolarization, *Ann. Geophys.*, **23**, 2915–2920, doi:10.5194/angeo-23-2915-2005.
- Nakamura, R., A. Retinò, W. Baumjohann, M. Volwerk, N. Erkaev, B. Klecker, E. A. Lucek, I. Dandouras, M. André, and Y. Khotyaintsev (2009), Evolution of dipolarization in the near-Earth current sheet induced by earthward rapid flux transport, *Ann. Geophys.*, **27**, 1743–1754, doi:10.5194/angeo-27-1743-2009.
- Olson, J. V. (1999), Pi2 pulsations and substorm onsets: A review, *J. Geophys. Res.*, **104**, 17,499–17,520, doi:10.1029/1999JA900086.
- Panov, E. V., et al. (2010), Multiple overshoot and rebound of a bursty bulk flow, *Geophys. Res. Lett.*, **37**, L08103, doi:10.1029/2009GL041971.
- Pontius, D. H. Jr., and R. A. Wolf (1990), Transient flux tubes in the terrestrial magnetosphere, *Geophys. Res. Lett.*, **17**, 49–52, doi:10.1029/GL017i001p00049.
- Pytte, T., R. L. McPherron, M. G. Kivelson, H. I. West Jr., and E. W. Hones Jr. (1976), Multiple-satellite studies of magnetospheric substorms—Radial dynamics of the plasma sheet, *J. Geophys. Res.*, **81**, 5921–5933, doi:10.1029/JA081i034p05921.
- Raeder, J., J. Berchem, and M. Ashour-Abdalla (1998), The geospace environment modeling grand challenge: Results from a global geospace circulation model, *J. Geophys. Res.*, **103**, 14,787–14,798, doi:10.1029/98JA00014.
- Raeder, J., R. L. McPherron, L. A. Frank, S. Kokubun, G. Lu, T. Mukai, W. R. Paterson, J. B. Sigwarth, H. J. Singer, and J. A. Slavin (2001), Global simulation of the geospace environment modeling substorm, *J. Geophys. Res.*, **106**, 381–395, doi:10.1029/2000JA000605.
- Runov, A., V. Angelopoulos, M. I. Sitnov, V. A. Sergeev, J. Bonnell, J. P. McFadden, D. Larson, K.-H. Glassmeier, and U. Auster (2009), THEMIS observations of an earthward-propagating dipolarization front, *Geophys. Res. Lett.*, **36**, L14106, doi:10.1029/2009GL038980.
- Runov, A., et al. (2011), Dipolarization fronts in the magnetotail plasma sheet, *Planet. Space Sci.*, **59**, 517–525, doi:10.1016/j.pss.2010.06.006.
- Russell, C. T., and R. L. McPherron (1973), The magnetotail and substorms, *Space Sci. Rev.*, **15**, 205–266, doi:10.1007/BF00169321.
- Saito, T., K. Yumoto, and Y. Koyama (1976), Magnetic pulsation Pi2 as a sensitive indicator of magnetospheric substorm, *Planet. Space Sci.*, **24**, 1025–1029, doi:10.1016/0032-0633(76)90120-3.
- Saito, T., and S. Matsushita (1968), Solar cycle effects on geomagnetic Pi2 pulsations, *J. Geophys. Res.*, **73**, 267–286, doi:10.1029/JA073i001p00267.
- Sakurai, T., and T. Saito (1976), Magnetic pulsations Pi2 and substorm onset, *Planet. Space Sci.*, **24**, 573–575, doi:10.1016/0032-0633(76)90135-5.
- Scholer, M., B. Klecker, D. Hovestadt, G. Gloeckler, F. M. Ipavich, and E. J. Smith (1984), Fast moving plasma structures in the distant magnetotail, *J. Geophys. Res.*, **89**, 6717–6727, doi:10.1029/JA089iA08p06717.



- Sergeev, V. A., V. Angelopoulos, J. T. Gosling, C. A. Cattell, and C. T. Russell (1996), Detection of localized, plasma-depleted flux tubes or bubbles in the midtail plasma sheet, *J. Geophys. Res.*, *101*, 10,817–10,826, doi:10.1029/96JA00460.
- Sitnov, M. I., M. Swisdak, and A. V. Divin (2009), Dipolarization fronts as a signature of transient reconnection in the magnetotail, *J. Geophys. Res.*, *114*, A04202, doi:10.1029/2008JA013980.
- Slavin, J. A., et al. (1997), WIND, GEOTAIL, and GOES 9 observations of magnetic field dipolarization and bursty bulk flows in the near-tail, *Geophys. Res. Lett.*, *24*, 971–974, doi:10.1029/97GL00542.
- Southwood, D. J., and W. F. Stuart (1980), Pulsations at the substorm onset, in *Dynamics of the Magnetosphere*, edited by S.-I. Akasofu, pp. 341–355, D. Reidel, Dordrecht, The Netherlands.
- Sutcliffe, P. R. (1975), The association of harmonics in Pi2 power spectra with the plasmapause, *Planet. Space Sci.*, *23*, 1581–1587, doi:10.1016/0032-0633(75)90085-9.
- Sutcliffe, P. R., and K. Yumoto (1991), On the cavity mode nature of low-latitude Pi2 pulsations, *J. Geophys. Res.*, *96*, 1543–1551, doi:10.1029/90JA02007.
- Takahashi, K., S.-I. Ohtani, and K. Yumoto (1992), AMPTE CCE observations of Pi2 pulsations in the inner magnetosphere, *Geophys. Res. Lett.*, *19*, 1447–1450, doi:10.1029/92GL01283.
- Walker, R. J., M. Ashour-Abdalla, M. El Alaoui, and F. V. Coroniti (2006), Magnetospheric convection during prolonged intervals with southward interplanetary magnetic field, *J. Geophys. Res.*, *111*, A10219, doi:10.1029/2005JA011541.
- Wolf, R. A., Y. Wan, X. Xing, J.-C. Zhang, and S. Sazykin (2009), Entropy and plasma sheet transport, *J. Geophys. Res.*, *114*, A00D05, doi:10.1029/2009JA014044.
- Yeoman, T. K., and D. Orr (1989), Phase and spectral power of mid-latitude Pi2 pulsations—Evidence for a plasmaspheric cavity resonance, *Planet. Space Sci.*, *37*, 1367–1383, doi:10.1016/0032-0633(89)90107-4.